Questing for an optimal, universal viral agent for oncolytic virotherapy

L. R. Paiva,[*] M. L. Martins,[†] and S. C. Ferreira[‡]

Departamento de Física, Universidade Federal de Viçosa, 36570-000 Viçosa, Minas Gerais, Brazil

One of the most promising strategies to treat cancer is attacking it with viruses designed to exploit specific altered pathways. Here, the effects of oncolytic virotherapy on tumors having compact, papillary, and disconnected morphologies are investigated through computer simulations of a multiscale model coupling macroscopic reaction-diffusion equations for the nutrients with microscopic stochastic rules for the actions of individual cells and viruses. The interaction among viruses and tumor cells involves cell infection, intracellular virus replication, and the release of new viruses in the tissue after cell lysis. The evolution over time of both the viral load and cancer cell population, as well as the probabilities for tumor eradication, were evaluated for a range of multiplicities of infection, viral entries, and burst sizes. It was found that in immunosuppressed hosts, the antitumor efficacy of a virus is primarily determined by its entry efficiency, its replicative capacity within the tumor, and its ability to spread over the tissue. However, the optimal traits for oncolytic viruses depend critically on the tumor growth dynamics and do not necessarily include rapid replication, cytolysis, or spreading, currently assumed as necessary conditions for a successful therapeutic outcome. Our findings have potential implications on the design of new vectors for the viral therapy of cancer.

PACS number(s): 87.19.xj, 87.10.Mn, 87.18.Hf

I. INTRODUCTION

Despite the progress that has been made in the imaging, diagnosis, treatment, and understanding of cancer, the survival rates of patients with metastatic or recurrent neoplasias as well as patients with tumors at unresectable locations are still poor, and new therapeutic strategies are needed [1]. Furthermore, occult, dormant micrometastases raise new challenges concerning their reactivation and evolution into clinically manifested disease, particularly after primary tumor resection [2].

Oncolytic virotherapy is a promising anticancer strategy because it can provide locoregional control or even eradication of tumors without cross-resistance with standard therapies. Oncolytic viruses are able to selectively infect and kill tumor cells by exploiting the same cellular defects that promote tumor growth [3]. To date, several different viruses are known to be selectively oncolytic [4]. An archetype is the adenovirus commonly used in gene therapy and oncolytic therapy experiments [5,6]. Some studies indicate that the virus effectiveness strongly depends on the specific cancer cell line [1]. Therefore, one can hypothesize that for each tumor there must exist an oncolytic virus that maximizes the therapeutic success.

Several mathematical models have been proposed to study virotherapy [7–10]. They have emerged as valuable tools to provide a quantitative understanding of the major mechanisms that affect anticancer treatments based on viruses and to select parameter ranges that enhance therapeutic success. These models are particularly valuable because, in the face of the nonlinearities and complexity involved in cancer progression and its interaction with oncolytic viruses, intuitive reasoning alone may be insufficient. The current paradigm is that the viral life cycle should lead to rapid replication, cytolysis, and spread [11]. Nonetheless, the limitations and validity of this appealing, intuitive, and seemingly logical paradigm remain unclear. Indeed, at least one mathematical result [8] indicates that viruses able to destroy tumor cells very quickly do not necessarily lead to a more effective control of tumor growth. More precisely, it was shown that successful virotherapy of compact tumors requires both highly spreading viruses and an optimal range of viral cytotoxy, i.e., neither too short nor a very long time for the lysis of cancer cells. However, this result was derived assuming that the viruses are a continuous field with dynamics described by a reaction-diffusion equation. Furthermore, the changes in the stationary local concentrations of viruses due to their entry at cell infections were neglected, and the viral-burst size used, equal to the initial viral load, was orders of magnitude greater than those of the larger ones observed for real oncolytic viruses.

In the present paper, a multiscale model based on the approach proposed by Ferreira *et al.* [12] was modified to take explicitly into account the individual, discrete nature of the oncolytic viruses and was applied to evaluate the efficacy of virotherapy against compact, papillary, and diffuse (disconnected) solid tumors. Considering viruses as discrete agents provides a more realistic description of virus entry and replication, key processes involved in oncolytic virotherapy. Our main goal is to provide useful insights concerning how to match the oncolytic virus and the tumor type in order to get the best outcome for a therapy.

II. MODEL

Figure 1 illustrates the multiple agents and processes involved in the model at distinct time and length scales. The tissue is modelled by a square lattice fed through a single capillary vessel at its top. Four different cell types (normal and dead cells and uninfected and infected tumor cells) and

———————
[*]leticia.paiva@ufv.br
[†]National Institute of Science and Technology for Complex Systems, Brazil; mmartins@ufv.br
[‡]On leave at the Departament de Física y Enginyeria Nuclear, Universitat Politécnica de Catalunya, Spain.
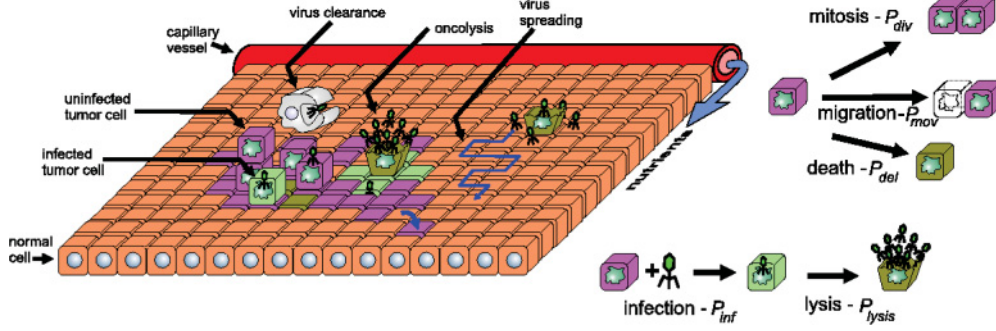
FIG. 1. (Color online) Schematic illustration of the mathematical approach. The model considers normal cells, tumor cells, and oncolytic viruses. Uninfected cancer cells can replicate by mitosis, die due to starvation (lack of nutrients), move, or become infected, a quiescent state in which the cellular machinery is slaved to promote viruses replication. Cell actions are stochastically governed by the probabilities P_{div}, P_{del}, P_{mov}, and P_{inf}, dependent on the nutrient and virus concentrations per cancer cell. Infected cancer cells die by lysis with the probability P_{lysis}. After mitosis, the new tumor cells can either pile up (loss of contact inhibition) at the site of parent cells or randomly invade a normal or necrotic nearest-neighbor cell, if any exists. Nutrients are modelled as continuous concentrations which evolve in space (tissue) and time according to reaction-diffusion equations. Essentially, nutrients diffuse from the capillary vessel through the tissue and are taken up by normal and tumor cells at distinct rates. Free viruses perform Brownian motions (lattice diffusion) and are cleared at a rate γ_v. The source of new viruses is infected cancer cells, which release v_0 new viruses after undergoing lysis. The virus clearance rate represents the simplest way to introduce viral loss, due mainly to the innate and adaptive immune response mediated by antibodies, CD8 T cells, interferons, and other cytokines or to inherent viral instability.

an oncolytic virus are considered. These individual agents are described by their populations σ_n, σ_d, σ_c, and σ_v, respectively, at every site x. In contrast to the normal and dead cells, one or more uninfected or infected cancer cells can pile up at a given site, reflecting the fact that the division of tumor cells is not constrained by contact inhibition. In turn, since the viruses are very small particles in comparison with cells, there is no constraint on their population.

The nutrients, diffusing from the capillary vessel throughout the tissue, are divided into two groups: those that limits cell replication but are not demanded for cell survival ($j = 1$) and those essential to maintain the basic cell functions and whose deprivation can induce death ($j = 2$). Both nutrient types are described by continuous fields $\phi_j(\vec{x},t)$, which evolve in space and time according to the simplest (linear with constant coefficients) dimensionless reaction-diffusion equations:

$$\frac{\partial \phi_j}{\partial t} = \nabla^2 \phi_j - \alpha^2 \phi_j \sigma_n - \lambda_j \alpha^2 \phi_j \sigma_c. \tag{1}$$

The factors λ_j take into account distinct nutrient uptake rates for normal and cancer cells. The parameter α sets up a characteristic length scale for nutrient diffusion in the normal tissue (see Ref. [13] for the complete variable transformations leading to this dimensionless equation). Equation (1) obeys a periodic boundary condition along the direction parallel to the capillary and a Neumann boundary condition at the border of the tissue. At the capillary vessel, the nutrient concentrations are $\phi_j = 1$ (continuous and fixed supply).

Each uninfected cancer cell, randomly selected with equal probability, can carry out one of the following four actions.

A. Mitotic replication

Mitotic replication has a probability

$$P_{\text{div}} = 1 - \exp\left[-\left(\frac{\phi_1}{\theta_{\text{div}}\sigma_c}\right)^2\right], \tag{2}$$

an increasing function of the concentration per cancer cell of the nutrients ϕ_1 controlled by the parameter θ_{div}. A daughter cell randomly occupies one of its normal or necrotic nearest-neighbor sites, if any exists, or piles up at its mother site. In the simulations, we observed at most three or four cancer cells at the same site simultaneously.

B. Death

Death has a probability

$$P_{\text{del}} = \exp\left[-\left(\frac{\phi_2}{\theta_{\text{del}}\sigma_c}\right)^2\right], \tag{3}$$

a Gaussian distribution whose variance depends on the model parameter θ_{del} and that increases with the scarcity of nutrients ϕ_2 essential to sustain the cell metabolism.

C. Migration

Migration has a probability

$$P_{\text{mov}} = 1 - \exp\left[-\sigma_c\left(\frac{\phi_2}{\theta_{\text{mov}}}\right)^2\right], \tag{4}$$

which increases with the local population of cancer cells and the nutrient concentration per cell. The model parameter θ_{mov} controls the shape of this sigmoid. A probability increasing with the nutrient concentration is justified by the necessity of nutrients for cell motility and, in addition, by the degradation of the extracellular matrix near the tumor surface that releases several chemicals that promote cell migration and proliferation. This hypothesis is consistent with experimental data in multicellular tumor spheroids [14] and was previously used in other mathematical models [15,16]. The migrating cell moves to one of its nearest-neighbor sites chosen at random, interchanging its position with a normal or necrotic cell if any exists. If the interchanged normal or necrotic cell moves

to a site still occupied by other cancer cells, it is eliminated. These rules for cancer growth are similar to those used by Scalerandi *et al.* [17] in a deterministic model with collective cell actions controlled by threshold (step) functions of the nutrient concentration per cancer cell.

D. Infection

Infection has a probability

$$P_{\text{inf}} = 1 - \exp\left[-\left(\frac{\sigma_v}{\sigma_c \theta_{\text{inf}}}\right)^2\right], \tag{5}$$

an increasing function of the local viral load per cell, controlled by the parameter θ_{inf}. The model assumes perfect viral selectivity for cancer cells, and thereby the infection of normal cells by oncolytic viruses is neglected. The number of viruses n_v that infect a given cell is selected from a Poisson distribution

$$P(n_v) = \frac{k^{n_v} e^{-k}}{n_v!}, \tag{6}$$

where k is the typical viral entry. This Poisson law has been observed in cell cultures as a function of the multiplicity of infection (m), defined as the ratio of the total viral load injected in the system and the number of target cells [18]. The model assumes that an infected cancer cell does not divide nor migrate because its slaved cellular machinery is focused on virus replication. It is also assumed that infected cancer cells sustain their metabolism until lysis and die only by lysis. Death by lysis occurs with a probability

$$P_{\text{lysis}} = 1 - \exp\left(-\frac{T_{\text{inf}}}{T_l}\right), \tag{7}$$

where T_{inf} is the time elapsed since the cell infection and T_l is the characteristic time for cell lysis. The lysis of each infected cancer cell releases

$$v_0 = b_s \frac{n_v}{A + n_v} \tag{8}$$

free viruses into the extracellular medium. Here, the maximum virus burst size b_s and A are model parameters. At the time of lysis, the new free viruses remain at the site of the lysed cell. They diffuse independently through the tissue by performing lattice random walks comprising q steps and are cleared at a rate γ_v at each time step. The clearance rate γ_v embodies

the complex innate and adaptive immune responses to a virus. Such response involves the synthesis of antiviral cytokines, the activation and/or selection of immune cells, and the production of antiviral antibodies [19].

The tumor starts to grow from a single cancer cell, and the therapy begins when the tumor attains N_0 cells. It consists of a single direct intratumoral administration in which $N_0 \times m$ viruses are uniformly spread over the entire tumor. This approach corresponds to the experimental protocols used in severe combined immunodeficient (SCID) mice [20] and *in vitro* assays [21,22]. Indeed, in most *in vivo* virotherapy experiments, the viruses are injected directly into a subcutaneous, avascular tumor developed in the mice.

More details concerning the procedures used for model simulations are provided in Appendixes A and B.

III. RESULTS

We are interested in the effects of virotherapy on compact, papillary, and disconnected tumors and the general morphologies observed in solid malignant neoplasias. Typical patterns corresponding to such morphologies were simulated using the multiscale model for the growth of avascular tumors studied in Ref. [13]. They are shown in Fig. 2, and the model parameters used are listed in Table I.

Typical progress curves for cancer cells and free viruses in a simulated virotherapy of a diffuse tumor are shown in Fig. 3. Similar time evolutions are also observed for solid and papillary neoplastic morphologies (see Appendix C). Two regimes are observed; either the cancer cell population keeps growing after the virus administration, or both cancer cells and oncolytic viruses are eradicated. In the former regime in which the virotherapy fails, the viruses can be either eradicated or coexist with the tumor cells. Such coexistence can exhibit oscillations in cancer cells and virus populations due to successive rounds of infection unable to eliminate the tumor. As previously reported [8], it is worthwhile to emphasize that any of these behaviors can randomly emerge as the response of a given tumor to the virotherapy. Hence, it becomes imperative to determine for each tumor morphology the most probable prognosis after treatment as well as the chances for the occurrence of the other tumor responses as functions of the virotherapeutic parameters.
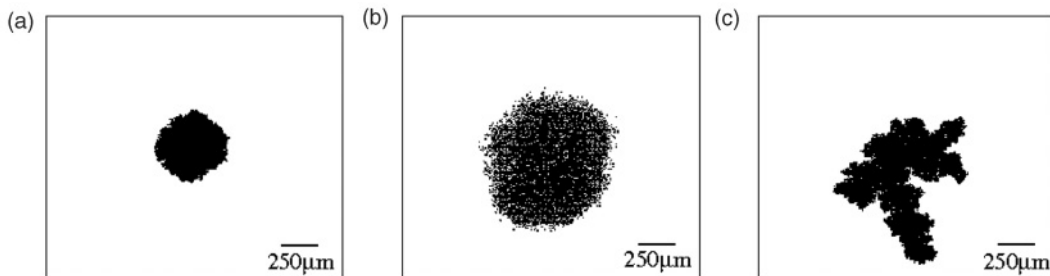

FIG. 2. Simulated morphologies for avascular tumor growth. (a) Solid or compact tumors grow exponentially fast under weak competition for nutrients and reduced cell motility. (b) Diffuse or disconnected tumors are characterized by a moderate level of nutrient competition and a high cell motility. (c) Papillary patterns emerge under strong nutrient competition and low cell motility, resulting in very slow growth. The parameters used are listed in Table I. All tumor patterns shown have 10^4 cells. The capillary is at the bottom of the frames.

TABLE I. Parameter values used in the simulations.

Tumor morphology	Parameter	Values	Description
	θ_{div}	0.3 (fixed)	Controls the probability of cancer cell division
	λ_2	10 (fixed)	Controls the competition for NE nutrients
Compact	θ_{del}	0.03	Controls the probability of cancer cell death
or			
solid	θ_{mov}	5	Controls the probability of cancer cell migration
	λ_1	25	Controls the competition for E nutrients
	α	0.02	Dimensionless nutrient uptake rate for normal cells
Papillary	θ_{del}	0.01	
or	θ_{mov}	5	
ramified	λ_1	200	
	α	0.06	
Disconnected	θ_{del}	0.01	
or	θ_{mov}	0.001	
diffuse	λ_1	50	
	α	0.06	
Viral traits	Parameter	Values	Description
	θ_{inf}	0.01 (fixed)	Determines the chance of virus infection (infectivity)
	γ_v	0.01 (fixed)	Virus clearance rate in the tissue
	A	0.5 (fixed)	Controls the number of viruses released after cell lysis
	m	1,1.5,5	Initial viral load (MOI) administered.
	k	1,1.5,5	Number of viruses entering a cell at infection
	b_s	10,50,100	Maximum number of viruses released after cell lysis
	q	1,4,9,16,25	Number of random steps performed by a virus per MCS
	T_l	2,4,8,16,32	Characteristic time for cell lysis

Abbreviations: NE and E, nonessential and essential for DNA replication and mitosis, respectively; MOI, multiplicity of infection; MCS, Monte Carlo or simulation time step.

Figure 4 shows the probabilities for the eradication of a papillary tumor. As one can see, a single intratumoral administration of an aggressive virus ($\theta_{\text{inf}} = 0.01$) with $m = 1.0$ and viral entry $k = 1.0$, a low clearance rate $\gamma_v = 0.03$, and $N_0 = 10\,000$ can eradicate the tumor. Even viruses with low replicative potential, associated with small burst sizes ($b_s = 10$, for instance), have almost 100% efficacy if they spread very slowly ($q \lesssim 4$) throughout the papillary tumor. As shown in Fig. 4(a), the antitumor efficacy of low-diffusive viruses depends very weakly on T_l, the characteristic time spent by the virus to induce the lysis of infected cancer cells. Furthermore, the antitumor efficacy decreases rapidly

with the increase of the virus diffusivity, almost vanishing for $q \gtrsim 9$. In contrast, for a highly replicative virus (burst size $b_s = 100$), the tumor eradication is almost always certain. The exceptions are for highly cytolytic ($T_l \lesssim 10$) and diffusive ($q \gtrsim 20$) viruses. Indeed, as shown in Fig. 4(b), the probability of therapeutic success goes to zero if the oncolytic virus spreads very quickly in the tissue and quickly kills cancer cells.

Bearing in mind the current paradigm (fastest viral replication, cytolysis, and spreading), the correlations revealed here among therapeutic outcomes and the traits of the antitumor vectors demonstrate a counterintuitive scenario. Indeed, a
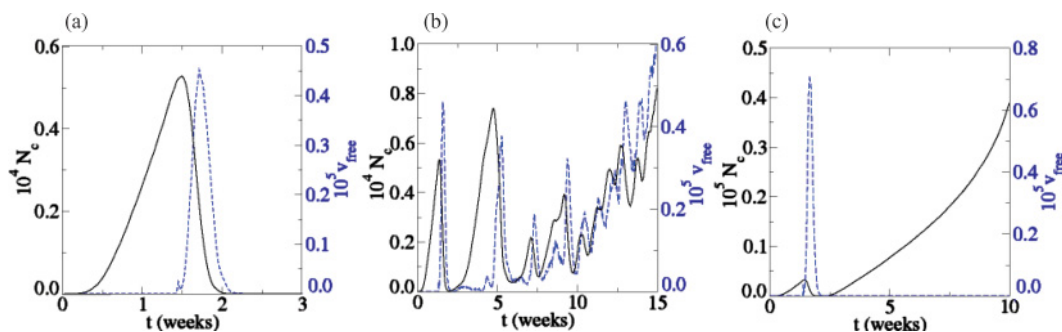

FIG. 3. (Color online) Temporal evolution of uninfected cancer cells (solid black line) and free-virus populations (dashed blue line) in a diffuse tumor. A single intratumoral virus load was administered when the tumor had $N_0 = 5000$ cells. Notice that three different behaviors were obtained using exactly the same fixed set of parameters and initial conditions ($m = 1$, $bs = 100$, $k = 1$, $q = 25$, and $T_l = 16$). These different behaviors emerge from stochasticity. The parameters used are listed in Table I.
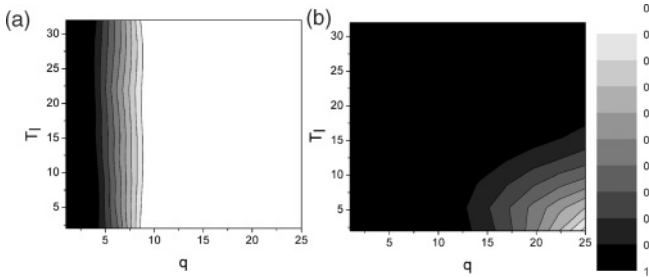
FIG. 4. (Color online) Papillary tumor eradication probability for distinct virus diffusivities q and time for lysis T_l. Two viral-burst sizes (a) $b_s = 10$ and (b) $b_s = 100$ are shown. The values $\gamma_v = 0.03$, $\theta_{inf} = 0.01$, $m = k = 1$, and $N_0 = 10^4$ are fixed. The probabilities were evaluated from 50 independent samples.

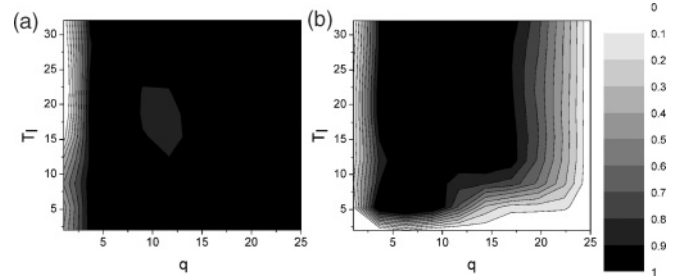

FIG. 5. Solid tumor eradication probability as a function of the parameters q and T_l. (a) $m = 1$ and viral entry $k = 5$ and (b) $m = k = 1.5$. The viral-burst size is $b_s = 100$, and the values $\gamma_v = 0.03$, $\theta_{inf} = 0.01$, and $N_0 = 5000$ are fixed. The probabilities were evaluated from 50 independent samples for each pair (q, T_l).

low viral diffusivity, independent of the cytolytic period T_l and replicative capacity b_s, is sufficient because papillary malignant neoplasias grow slowly. Nonetheless, one can argue that viruses exhibiting low diffusion rates in tissues will hardly reach the tumor if intravenously or systemically administered. Hence, this trait should be clinically avoided unless delivery barriers have been overcome through some "prodiffusive" strategy. As an alternative, our results indicate that quickly spreading viruses combining high replication potentials and slow cytolysis can successfully eliminate papillary tumors.

The aforementioned results should be compared with those obtained for a compact tumor in order to determine if the most effective virus against papillary tumors is equally efficient in the treatment of compact tumors. Compact morphologies are generated in our model when competition for nutrients is weak, and consequently, the tumor grows quickly. The same oncolytic virus and treatment protocol successfully used for papillary tumors ($\gamma_v = 0.03$, $\theta_{inf} = 0.01$, $m = 1$, $k = 1$, and $N_0 = 10\,000$) fails for compact tumors. They are not eradicated for any T_l and q values studied even for a large burst size ($b_s = 100$). Therefore, very efficient viruses against papillary tumors can be ineffective to eradicate compact tumors. While the number of cancer cells increases, the viruses either become extinct, if $q = 1$, or coexist with the growing tumor, if $q > 1$. In the coexistence regime, the tumor grows continuously but at a slower rate.

Given that solid tumors grow faster than ramified ones, it seems intuitive to assume that more diffusive viruses might be more effective against the neoplastic mass. However, the success probabilities remain null when only the viral diffusivity is increased up to values as large as $q = 900$. One alternative for a successful therapy is to reinforce the viral load initially administered. Nonetheless, even at larger m ($m = 5$, for instance) the therapy still completely fails if the viral entry $k = 1$ is maintained. The value $k = 1$ implies that on average only one virus invades a cell at each infection event.

A remaining strategy to control compact tumor growth is to enhance the viral entry. As one can see in Fig. 5(a), a large viral entry ($k = 5$) has a dramatic effect on the therapeutic success. Indeed, the virotherapy only fails, even using $m = 1$, for very low viral diffusivities ($q \leqslant 2$) and large lytic periods ($T_l \gtrsim 15$). Furthermore, significant success is achieved by

reducing k while, on balance, increasing the m used. This is shown in Fig. 5(b) in which $k = 1.5$ and $m = 1.5$. In this case, a successful therapy demands an oncolytic virus with an appropriate diffusivity and lytic cycle. An adequate diffusion ($3 \lesssim q \lesssim 16$) allows viral spreading throughout the compact tumor at a rate similar to or greater than that of the growing neoplasia. However fixed the viral diffusivity, the time T_l must lie within a certain range, such as, for instance, $7 \lesssim T_l \leqslant 32$ for $q = 15$. Indeed, a very rapid cytolysis promptly forms "voids" containing the majority of the newly released viruses, which impair the generation of new infection waves. In turn, a very long T_l generates successive waves of infection at a low frequency unable to destroy the tumor. These results are consistent with those reported in Ref. [8], supporting the robustness of both models.

Finally, the response of diffuse tumors to virotherapy was investigated. In our model, disconnected patterns emerge for highly motile cells that uptake nutrients at moderate rates. Considering an oncolytic virotherapy based on a viral agent with high replicative capacity, the probability for the eradication of a diffuse tumor is shown in Fig. 6. As one can see, the success probability also vanishes for highly diffusive viruses and
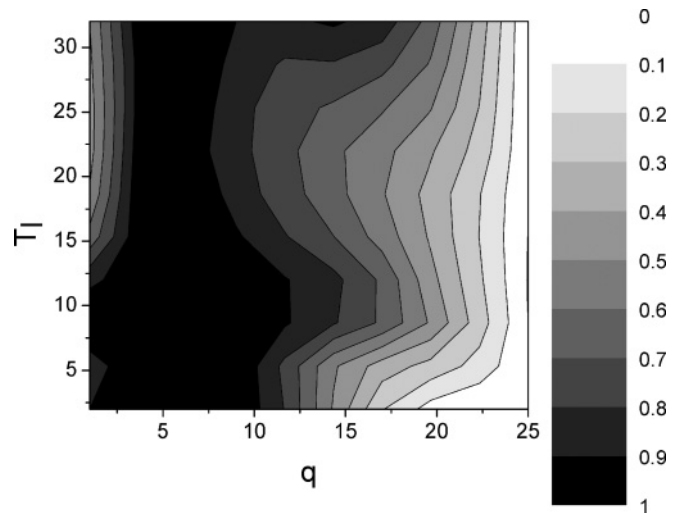

FIG. 6. Diffuse tumor eradication probability as a function of the parameters q and T_l. The viral-burst size $b_s = 100$ is used. The values $\gamma_v = 0.03$, $\theta_{inf} = 0.01$, $m = 1$, $k = 1$, and $N_0 = 10\,000$ are fixed.

increases significantly for viruses spreading slowly. Optimal oncolytic viruses to treat diffuse tumors should combine high replicative rates and intermediate diffusivity. If the virus has a slower rate of spreading, then a short time to induce the lysis of infected cancer cells is necessary in order to maximize the therapeutic success. At greater viral spreading ($8 \lesssim q \lesssim 16$), the success probability exhibits a reentrant behavior characterized by an initial decrease, followed by an increase of the therapeutic success as the cytolytic period T_l increases.

IV. DISCUSSION

In this work we investigated the oncolytic virotherapeutic outcomes for solid (compact, papillary, and diffuse) tumors using numerical simulations. We focused our study on vectors with high infectivities and small clearance rates, corresponding to a severe suppression of the host immune response. Furthermore, since in the present framework the discrete nature of the oncolytic virus allows a more realistic modeling of the viral infection and replication processes, the central roles of viral-burst size b_s, virus entry k, and initial m for the therapeutic success are highlighted.

Figure 3 illustrates our typical results. After a single intratumoral virus administration, these tumors can either be completely eradicated or will keep growing with time despite a transient remission, as per results previously obtained for compact tumors [8]. Furthermore, the latter behavior can be either a monotonic or an oscillating growth. It is worthwhile to note that such oscillations were observed in human myeloma xenografts induced in mice treated with the measles virus (MV) [23], in an ovarian cancer xenograft model [24], and in a mathematical approach used by Dingli *et al.* for modeling a MV virotherapy [25]. The therapeutic outcome depends on both viral characteristics and tumor dynamics. Therefore, for fixed viral infectivity θ_{inf} and persistence within the tissue determined by γ_v, the key parameters that control treatment success are the virus entry k, viral diffusivity q, characteristic lytic time T_l, and tumor growth rates.

Concerning the virotherapy of solid tumors, two main results deserve special attention. First, in the case of low virus entry ($k = 1$), successful therapeutic outcomes were observed only at large, but realistic, initial m values and viral-burst sizes. It must be mentioned that the viral-burst size used in Ref. [8], equal to the initial viral load, was one order of magnitude greater than those of the larger viral-burst sizes observed for real oncolytic viruses. In turn, the large initial m required by successful virotherapies in our present simulations with $k = 1$ raises the question of the clinical risks involved. Viral doses ranging from about 10^7 pfu (plaque-forming unit) ($m \approx 0.08$) to 10^9 pfu ($m \approx 8$) were used in experimental tests [26]. Also, it is known that the oncolytic adenovirus *dl1520* (or *ONYX-015*) is well tolerated at the higher practical, administered doses (2×10^{12}–2×10^{13} particles) [6]. However, at very high viral titer (about 1×10^{14} particles per kg), this virus caused the death of a gene therapy patient with ornithine-cystosine transferase deficiency [27]. Hence, the use of reduced viral doses is pursued in clinical applications, particularly in order to allow for systemic administration.

Successful outcomes could be accomplished by raising the viral entry k (see Fig. 5). Indeed, k represents the average number of viruses entering a cancer cell at infection. Thus, large values of k result in the high production of new viruses ($v_0 \sim b_s$, the viral-burst size) that are released after cell lysis. This local enhancement of the free-virus load increases, in turn, the probability of further cancer-cell infection. The consequence of such a positive feedback cycle is that the initial viral load is sufficient to trigger a powerful first wave of infection whose successive rounds end in destroying the tumor. Moreover, as shown in Fig. 5(b), a relatively slight and simultaneous increase of both the virus entry and m can be enough to guarantee a successful oncolytic treatment of compact tumors with safe viral doses.

Second, considering that large viral loads involve risks and that an elevated virus entry may represent a significant technical barrier, treatments based on intermediate m and k values become of special interest. In this range ($m \sim 1$ and $1 \leqslant k < 2$), the key factors determining the therapeutic success are viral diffusivity and cytolytic period. The probability of tumor eradication vanishes for viruses that diffuse very quickly even at large m. Indeed, a very rapid spreading disperses the viruses outside the growing tumor where they cannot trigger new waves of infection. In turn, since the growth of compact tumors is faster, an effective oncolytic virus must not diffuse more slowly than the tumor spreading. At intermediate values of k and m, in addition to being able to spread at a rate similar to that of the growing tumor, the virus must induce the lysis of infected cancer cells neither too slowly nor too quickly. If the time T_l for cytolysis is very short, voids containing the majority of the newly released viruses rapidly form throughout the tumor. These viruses cannot trigger new infection waves, and cancer cells at the border of some voids escape. In turn, if T_l is very long, the successive waves of infection are generated at a low frequency, too separated in time to destroy the tumor. These findings are consistent with the predictions in Fig. 5 of Ref. [8] which suggests that the ideal oncolytic virus should have neither a very short nor a long lytic cycle.

Summarizing, a successful virotherapy of compact tumors demands the simultaneous optimization of several factors: the use of oncolytic viruses with high replicative capacities (burst sizes), adequate diffusivities (rapid but not too rapid spreading), and lytic cycle (neither too short nor too long) as well as a large initial viral entry. The importance of the initial m, strongly emphasized by Demers *et al.* [28] and Myers *et al.* [23], is much less than that associated with the virus entry. In those experiments, huge variations in the initial viral load, from 10^4 to 10^{10} viral particles, were performed. Such values correspond to an m value ranging from around 0.5 to about 500. As one can intuitively expect, our simulations evidence that a huge m eradicates the tumor independent of other factors (viral traits and tumor growth dynamics). However, for virotherapies based on low virus entries and m there is, with a fixed viral diffusivity, an optimal range for its lytic-cycle period because the virotherapy fails if the cytolysis is either too short or too long. This result is in complete agreement with the findings of Paiva *et al.* [8]. Furthermore, we point out that the virotherapeutic efficacy is much more sensitive

to other parameters, for instance viral entry and burst size, than to m.

Regarding papillary tumors, a virotherapy based on small virus entry ($k = 1$) and initial viral load ($m = 1$) can control cancer growth. In this case the key factors determining a successful therapeutic outcome are the virus spreading and its replicative ability. Indeed, for small viral-burst sizes, the therapeutic outcome for papillary tumors is almost independent of T_l. We find that the virotherapy fails for oncolytic viruses with high diffusivities. Success probabilities greater than 70% are observed only for very small diffusivities ($q \lesssim 6$). In contrast, for a fixed diffusivity, the therapeutic success of highly replicative viruses exhibits a reentrant behavior as a function of their lytic periods as shown in Fig. 4(b). Again, our simulations suggest an optimal range for the time T_l demanded by the oncolytic virus to kill an infected tumor cell.

Finally, for fixed small virus entry ($k = 1$) and initial viral load ($m = 1$), optimal oncolytic viruses to treat diffuse tumors should exhibit high replicative rates and intermediate diffusivities. For faster viral spreading ($q \gtrsim 8$), a successful therapeutic outcome has a complex dependence on T_l. A reentrant behavior is observed, leading to a decreasing probability of success at an intermediate range of the time T_l for cytolysis. In contrast, for oncolytic viruses having much slower spreading rates, highly successful therapies require short times to induce the lysis of infected cancer cells.

A relevant issue is how our simulation results can be compared with those obtained from experimental assays of or clinical trials on oncolytic virotherapy. Unfortunately, this represents a difficult task due to the scarcity of quantitative experimental data. Most of the studies on oncolytic virotherapy have focused primarily on the safety of these vectors and evaluate the anticancer efficacy of viruses. Tests *in vitro* involve cancer cells cultured in monolayer or three-dimensional compact-tumor spheroid models. Either the xenograft models in experimental animals or the human tumors treated in clinical trials are also solid tumors with compact morphologies. Furthermore, since very distinct tumors were treated using several different viruses, both the system and the therapeutic conditions varied widely. Hence, almost all parameters have changed simultaneously from one experiment to another. Basically, the results are qualitative: the antitumor efficacy of viruses has been limited. Virotherapy is impaired by multiple factors, particularly low viral loads, suboptimal delivery to target sites, barriers to virus spreading within tumors, and the host immune response against these vectors.

Our simulations reveal that the virus entry k is the major parameter determining the therapeutic outcome. Once its value is fixed, the lower is the initial dose of virus administered, and the smaller is the chance of tumor eradication. Experimental [23] and mathematical [25] results support this direct correlation between m and therapeutic success. Also, our simulations indicate that virus replication within the tumor tissue, modelled by the viral-burst size b_s, is the next main trait in the hierarchy of factors determining virotherapeutic success. Such findings are supported by observations from Friedman *et al.* [7]. Decreasing within the hierarchy, the viral diffusivity emerges as the next key parameter for a successful virotherapy.

Experimental observations reporting that antitumor efficacy increases as intratumoral virus spreading is enhanced due to voids and channels generated by induced-cancer-cell apoptosis inside a tumor [29] are in agreement with this result. Finally, experimental data that confronts our results concerning the effects of the cytolytic time on the therapeutic outcome are lacking.

From our model simulations, the efficiency of virus entry in a cell, its replicative capacity inside an infected cell, and its diffusivity within the tumor tissue emerge as three crucial factors to fuel and amplify the successive rounds of infection necessary to control or eradicate the tumor. Hence, it is worthwhile to briefly comment on some trends of the experimental research in these directions. Concerning virus entry, a major challenge is the engineering of entry proteins to achieve higher levels of infectivity. But this approach is diametrically opposite to the search for entry inhibitors, neutralizing antibodies, and vaccine immunogens that elicit antibodies against virus-entry proteins [30,31]. Instead of fighting a virus, the goal is to transform it into a better entry machine while reinforcing its retargeting specificity. Here, experimental results are scarce and constrained to comparative analysis of the infectivities of distinct oncolytic viruses. Thus, for instance, Ketola *et al.* [1] compared the oncolysis in five human osteosarcoma cell cultures infected with the Semliki Forest virus *VA7-EGFP* and the adenovirus *Ad5Δ24*. They found that the kinetics of adenovirus infection were much slower than those of the Semliki Forest virus. Large amounts of adenoviruses were required to assure its spread throughout the cell cultures and to lyse all the osteosarcoma cells. Also, the authors demonstrated the differential efficacy of the Semliki Forest virus against human osteosarcoma cell lines. Virus spreading was observed in four of five cell lines studied. In particular, the cell lineage *MG-63* seemed to be relatively resistant to the *VA7-EGFP* infection. Clearly, these results can be understood in terms of the differences in virus entry and replicative capacities as evidenced in our model. Also, some attempts to enhance the replication of oncolytic viruses have been performed since, for instance, the burst size of a wild-type *HSV* is one or two orders of magnitude greater than that of the engineered vector *hrR3*. Alternatives include placing viral genes under the transcriptional control of tumor-specific promoters [32] and mutating viruses to express genes that overcome tumor-cell pathways blocking viral protein synthesis [33]. Again, more attention needs to be paid to this approach. A greater activity is observed in the field of virus spreading. Several vasoactive cytokines, or physical treatments, such as radiation or heat, increase tumor vessels permeability and blood flow, leading to faster diffusion [34]. Such strategies can be particularly relevant for systemic virus administration and in treating tumors at the vascular stage, mainly compact tumors exhibiting fast growth as our results indicate. The incorporation of lytic enzymes, such as hyaluronidase, into a conditionally replicative adenovirus could also increase diffusion rates [35]. Furthermore, agents that decrease the glycosaminoglycan concentration [36] or that degrade interstitial collagen [37,38] can improve transport in tumors. For instance, tumor collagen can significantly hinder diffusion, and it was shown [36] that the matrix metalloproteinases-1 and -8 can modulate the tumor matrix and

improve the distribution of an oncolytic virus throughout the tumor without affecting cell proliferation or viral replication. In addition, a previous work [39] showed that the matrix metalloproteinase-8 is antimetastatic, so it could be safely used to improve the viral diffusion in tumors. Strategies that change the tumor microenvironment are particularly important in enhancing the efficacy of virotherapies against avascular tumors and occult dormant metastases.

V. CONCLUSIONS

In summary, the outcomes of oncolytic virotherapies on solid tumors were investigated through computer simulations of a multiscale model for cancer growth. The model combines macroscopic diffusion equations for the nutrients and stochastic rules for the actions of individual cells and viruses. Our simulations reveal that in immunosuppressed hosts, the antitumor efficacy of a virus is determined primarily by its efficiency of entry, its replicative capacity within the cancer cell, and its ability to spread throughout the tissue. However, the balance between these viral traits depends on the tumor morphology. Indeed, the virotherapy of papillary tumors based on oncolytic viruses with small diffusivities is highly effective (success probability $\geqslant 80\%$) even for small virus entry but high replication capacity. Furthermore, the therapy fails if the virus both spreads and lyses infected cells very rapidly. In contrast, for compact tumors, the therapy fails if vectors characterized by small virus entry and slow intratumoral spreading are used at safe values of m. In turn, for diffuse tumors, an intermediate viral diffusivity maximizes the therapeutic success. Therefore, the design of efficient oncolytic viruses must take into account the dynamics of tumor growth, which is fast for compact but slow for papillary cancers. It is the tumor growth that determines the optimal traits for oncolytic viruses. These traits do not necessarily include high diffusivity and cytolysis, which are naively assumed as necessary conditions to amplify the therapeutic inoculum *in situ* and promote fast viral spreading throughout the affected tissue.

ACKNOWLEDGMENTS

APPENDIX A: SIMULATION PROTOCOL

The simulations were implemented as follows. At each time step, Eq. (1) is numerically solved in the stationary state ($\partial \phi / \partial t = 0$) through relaxation methods. Also, a fraction of the free virus present at every site is cleared, and each remaining virus performs an independent random walk with q steps. Provided the nutrient concentration and viral load at any lattice site, $N_c(t)$ cancer cells are sequentially selected at random with equal probability. (Here, $N_c(t)$ is the total number of tumor cells, uninfected or infected, at time t.) For each one of them, a tentative action (division, death, migration, or infection for an uninfected cancer cell and lysis for an infected one) is randomly chosen with equal probability. The selected cell action is implemented or not according to the corresponding local probabilities determined by Eqs. (2)–(5), and (7), and the time is incremented by $\Delta t = 1/N_c(t)$. If the carried action is the infection of the selected cell, an integer random number n_v distributed as a Poissonian is generated and compared with the local virus population σ_v. If $\sigma_v \geqslant n_v$, n_v viruses invade the uninfected cancer cell, decreasing σ_v by n_v. Otherwise, this process will be repeated until it generates $n_v \leqslant \sigma_v$. In turn, if the carried action is the lysis of the selected cell, v_0 new viruses are introduced at the site of the lysed cell. At the end of this sequence of $N_c(t)$ updates, a new time step starts, and the entire procedure (solution of the reaction-diffusion equations, virus clearance and spreading, and cell dynamics) is iterated. It is worthwhile to note that a particular cell can possibly perform more than one action in a certain time step, but on average every cancer cell will perform the same number of actions. Also, the increment time Δt assures that, on average, each cancer cell present at a given time has a chance to perform an action during that time step. The simulations stop if any tumor cell reaches the capillary vessel or the tissue border or if the tumor is eradicated ($N_c = 0$).

APPENDIX B: PARAMETER ESTIMATES

In all simulations, the tissue is represented by a square lattice of linear size $L = 500$ and lattice constant $\Delta = 10 \mu$m, corresponding to a tissue section of about 25 mm². Assuming a DNA synthesis phase of the cell cycle of about 11 h [40], one time step in the simulations corresponds to about 4–5 h. The parameters $\theta_{\rm div} = 0.3$ and $\lambda_2 = 10$ were fixed. In order to generate compact, papillary, and disconnected tumor growth
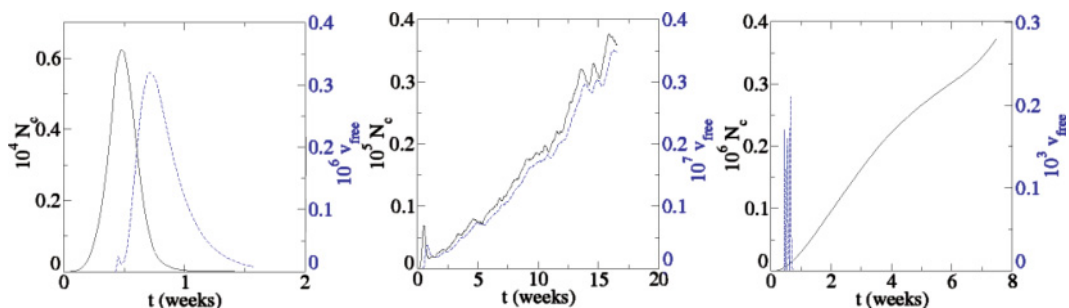

FIG. 7. (Color online) Progress curves—N_c (solid black line) and $v_{\rm free}$ (dashed blue line)—for compact tumors. The values $q = 4$, $T_l = 16$, $b_s = 100$, and $N_0 = 5000$ are used in all figures. In the case of tumor eradication, $m = 5$ and $k = 5$ are used. The coexistence of tumor cells and viruses is observed at $m = 1$ and $k = 1$. Finally, virus eradication occurs at $m = 0.01$ and $k = 0.01$.

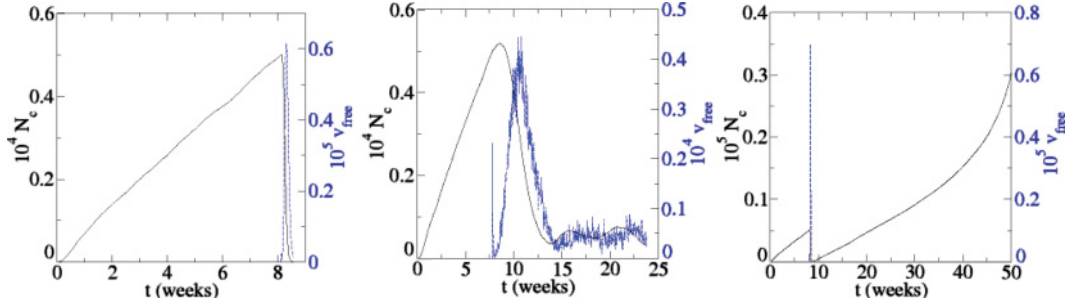FIG. 8. (Color online) Progress curves—N_c (solid black line) and v_{free} (dashed blue line)—for papillary tumors. The values $q = 25$, $T_l = 4$, $b_s = 100$, and $k = 1$ for the virus and $m = 1$ and $N_0 = 5000$ for the virotherapy are used.

patterns, distinct values of the parameters θ_{del}, θ_{mov}, λ_1, and α were used as listed in Table I. The parameters γ_v and θ_{inf}, characterizing the oncolytic virus, were also fixed (see Table I). The key parameters controlling virus diffusion q; entry k; replication b_s; the time for triggering cell lysis T_l; and m, specifying the virotherapy, were varied. The therapy begins when the tumors have either $N_0 = 5000$ or $10\,000$ cells.

The value fixed for γ_v, controlling viral clearance, is the same used in Ref. [8] and corresponds to a virus with a long residence time in the tissue (low clearance rate). In turn, the value $\theta_{\text{inf}} = 0.01$ corresponds to a highly infective oncolytic virus ($P_{\text{inf}} = 90\%$). Both of them are rather arbitrary, but for comparison, 70% of the $hr R3$ viruses successfully invade uninfected glioma cells [7]. The other viral parameters were varied in ranges biologically reasonable. Indeed, b_s ranged in the interval [10, 100] as experimentally observed for the burst size of the oncolytic virus $hr R3$ [7]. The m also varied within ranges used in virotherapy trials [26]. For comparison, viral doses ranging from about 10^7 pfu ($m \sim 0.08$) to 10^9 pfu ($m \sim 8$) were used in experimental tests [26]. The characteristic time for lysis T_l was varied as in Ref. [8]. Assuming a simulational time step of 4 h, T_l ranged from 8 h to 5 d. For comparison, the mean lifetime of glioma cells infected by $hr R3$ is ~ 18 h

[7], and the lytic cycle of the adenovirus $Ad2$ is 32–36 h. Therefore, the simulations assume viruses which are 4 times faster to 4 times slower than the $Ad2$. The values considered for the virus entry k lead, on average, to cell infections by few viruses simultaneously. Unfortunately, we could not find direct measures or estimates for k in the literature. Finally, q (the number of steps in a viral random walk), a measure of the viral spreading capacity, was estimated as follows. Since in a random walk $\langle r^2 \rangle = Dt$ or $\langle r^2 \rangle = q\Delta^2$, where D is the diffusion constant, t is the diffusion time, and Δ the length step, the virus diffusivity can be determined from q. Assuming $\Delta \sim 10\ \mu$m (lattice constant = linear cell size) and $t = 4$ h, one finds $D_{\text{min}} = 2.5 \times 10^{-5}$ mm^{2}h^{-1} for $q = 1$ and $D_{\text{max}} = 6.25 \times 10^{-4}$ mm^{2}h^{-1} for $q = 25$. These are the limit values used for the virus diffusivity in the simulations. Taking as a reference value $D = 1.8 \times 10^{-4}$ mm^{2}h^{-1}, the diffusivity of the HSV in tumors with high collagen content [41], D_{min} is ~ 14 times less than and D_{max} is ~ 3.5 times greater than this reference.

APPENDIX C

Here, additional results concerning the progress curves of viruses and uninfected cancer cells for compact and papillary tumors are shown in Figs. 7 and 8, respectively. Also, the effect of the viral-burst size for oncolytic agents characterized by moderate ($k = 2$) and high ($k = 5$) virus entry are exhibited in Figs. 9 and 10, respectively.
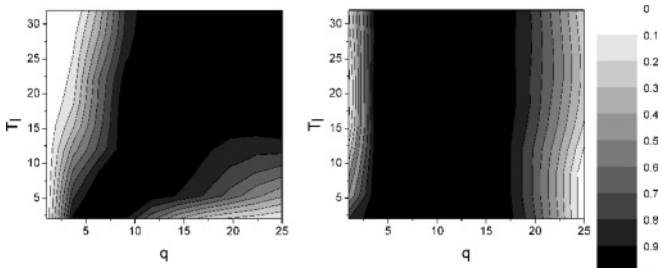

FIG. 9. The probability of success of a virotherapy applied to compact or solid tumors using $m = k = 2$. On the left $b_s = 10$, and on the right $b_s = 100$. $N_0 = 5000$ is fixed for the virotherapy. As can be noted, an unexpected coupling between T_l and b_s is observed. Indeed, for a large viral-burst size $b_s = 100$, the probability of success is practically independent of T_l. However, for a small value ($b_s = 10$), this probability decreases with increasing T_l for $q < 10$ (small viral spreading) but increases with T_l at larger q values. It seems that at a high diffusivity, even a virus with a low replicative capacity can sustain successive waves of infection by lysing the scattered cells that survive the previous rounds of infection.
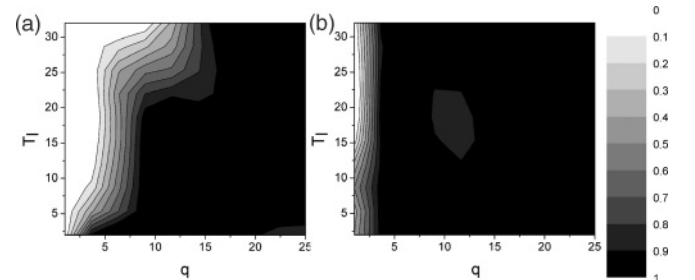

FIG. 10. The probability of success of a virotherapy applied to solid tumors using $m = 1$, $k = 5$, and $N_0 = 5000$. On the left $b_s = 10$, and on the right $b_s = 100$. Notice that the therapeutic success decreases only for a virus with very low spreading, particularly when its replicative capacity is low as well.

[1] A. Ketola, A. Hinkkanen, F. Yongabi, P. Furu, A. M. Maatta, T. Liimatainen, R. Pirinen, M. Bjorn, T. Hakkarainen, K. Makinen, J. Wahlfors, and R. Pellinen, Cancer Res. **68**, 8342 (2008).

[2] G. N. Naumov, J. Folkman, O. Straume, and L. A. Akslen, APMIS **116**, 569 (2008).

[3] T. C. Liu and D. Kirn, Gene Ther. **15**, 877 (2008).

[4] K. J. Harrington, R. G. Vile, and H. S. Pandha, *Viral Therapy of Cancer* (Wiley, Chichester, England, 2008).

[5] M. Yamamoto and D. T. Curiel, Mol. Ther. **18**, 243 (2010).

[6] K. Relph, K. J. Harrington, A. Melcher, and H. S. Pandha, in *Viral Therapy of Cancer*, edited by K. J. Harrington, R. G. Vile, and H. S. Pandha (Wiley, Chichester, 2008), pp. 1–17.

[7] A. Friedman, J. P. Tian, G. Fulci, E. A. Chiocca, and J. Wang, Cancer Res. **66**, 2314 (2006).

[8] L. R. Paiva, C. Binny, S. C. Ferreira Jr., and M. L. Martins, Cancer Res. **69**, 1205 (2009).

[9] D. Wodarz and N. Komarova, PLoS One **4**, e4271 (2009).

[10] C. Reis, J. Pacheco, M. Ennis, and D. Dingli, Integr. Biol. **2**, 41 (2010).

[11] K. A. Parato, D. Senger, P. A. J. Forsyth, and J. C. Bell, Nat. Rev. Cancer **5**, 965 (2005).

[12] S. C. Ferreira, M. L. Martins, and M. J. Vilela, Physica A **345**, 591 (2005).

[13] S. C. Ferreira Jr., M. L. Martins, and M. J. Vilela, Phys. Rev. E **65**, 021907 (2002).

[14] J. D. Freyer and P. L. Schor, J. Cell. Physiol. **138**, 384 (1989).

[15] A. R. Kansal, S. Torquato, G. R. Harsh IV, E. A. Chiocca, and T. S. Deisboeck, J. Theor. Biol. **203**, 367 (2000).

[16] I. Ramis-Conde, M. A. J. Chaplain, and A. R. A. Anderson, Math. Comput. Model. **47**, 533 (2008).

[17] M. Scalerandi, A. Romano, G. P. Pescarmona, P. P. Delsanto, and C. A. Condat, Phys. Rev. E **59**, 2206 (1999).

[18] *Cell Culture Technology for Pharmaceutical and Cell-Based Therapies*, edited by S. S. Ozturk and W.-S. Hu (CRC Press, Boca Raton, FL, 2006).

[19] R. Weinberg, *The Biology of Cancer* (Garland Science, New York, 2007).

[20] M. C. Coffey, J. E. Strong, P. A. Forsyth, and P. W. K Lee, Science **282**, 1332 (1998).

[21] J. R. Bischoff, D. H. Kim, A. Williams, C. Heise, S. Horn, M. Muna, L. Ng, J. A. Nye, A. Sampson-Johannes, A. Fattaey, and F. McCormick, Science **274**, 373 (1996).

[22] K. Raj, P. Ogston, and P. Beard, Nature (London) **412**, 914 (2001).

[23] R. M. Myers, S. M. Greiner, M. E. Harvey, G. Griesmann, M. J. Kuffel, S. A. Buhrow, J. M. Reid, M. Federspiel, M. M. Ames, D. Dingli, K. Schweikart, A. Welch, A. Dispenzieri, K. W. Peng, and S. J. Russell, Clin. Pharmacol. Ther. (NY, NY, US) **82**, 700 (2007).

[24] K. W. Peng, E. M. Hadac, B. D. Anderson, R. Myers, M. Harvey, S. M. Greiner, D. Soeffker, M. J. Federspiel, and S. J. Russell, Cancer Gene Ther. **13**, 732 (2006).

[25] D. Dingli, C. Offord, R. Myers, K. W. Peng, T. W. Carr, K. Josic, S. J. Russell, and Z. Bajzer, Cancer Gene Ther. **16**, 873 (2009).

[26] M. F. Ziauddin and D. Bartlett, in *Viral Therapy of Cancer*, edited by K. J. Harrington, R. G. Vile, and H. S. Pandha (Wiley, Chichester, 2008), pp. 151–69.

[27] S. Lehrman, Nature (London) **401**, 517 (1999).

[28] G. W. Demers, D. E. Johnson, V. Tsai, S. F. Wen, E. Quijano, T. Machemer, J. Philopena, M. Ramachandra, J. A. Howe, P. Shabram, R. Ralston, and H. Engler, Cancer Res. **63**, 4003 (2003).

[29] S. Nagano, J. Y. Perentes, R. K. Jain, and Y. Boucher, Cancer Res. **68**, 3795 (2008).

[30] D. S. Dimitrov, Nat. Rev. Microbiol. **2**, 109 (2004).

[31] D. M. Eckert and P. S. Kim, Annu. Rev. Biochem. **70**, 777 (2001).

[32] R. Y. Chung, Y. Saeki, and E. A. Chiocca, J. Virol. **73**, 7556 (1999).

[33] M. Mulvey, J. Poppers, D. Sternberg, and I. Mohr, J. Virol. **77**, 10917 (2003).

[34] R. K. Jain, Cancer Res. **50**, 814 (1990).

[35] R. Alemany, C. Balagué, and D. T. Curiel, Nat. Biotechnol. **18**, 723 (2000).

[36] W. Mok, Y. Boucher, and R. K. Jain, Cancer Res. **67**, 10664 (2007).

[37] P. A. Netti, D. A. Berk, M. A. Swartz, A. J. Grodzinsky, and R. K. Jain, Cancer Res. **60**, 2497 (2000).

[38] E. Brown, T. McKee, E. diTomaso, A. Pluen, B. Seed, Y. Boucher, and R. K. Jain, Nat. Med. (NY, NY, US) **9**, 796 (2003).

[39] V. Montel, J. Kleeman, D. Agarwal, D. Spinella, K. Kawai, and D. Tarin, Cancer Res. **64**, 1687 (2004).

[40] D. A. Rew and G. D. Wilson, Eur. J. Surg. Oncol. **26**, 405 (2000).

[41] W. Mok, T. Stylianopoulos, Y. Boucher, and R. K. Jain, Clin. Cancer Res. **15**, 2352 (2009).